

Dynamics of Phase Transitions: The 3D 3-state Potts Model

Bernd A. Berg^{a,b}, Hildegard Meyer-Ortmanns^d and Alexander Velytsky^{a,b}
(E-mails: berg@hep.fsu.edu, h.ortmanns@iu-bremen.de, velytski@csit.fsu.edu)

^{a)} Department of Physics, Florida State University, Tallahassee, FL 32306

^{b)} School of Computational Science, Florida State University, Tallahassee, FL 32306

^{d)} School of Engineering and Science, International University Bremen, P.O. Box 750561, D-28725 Bremen, Germany

(Dated: October 5, 2018)

In studies of the QCD deconfining phase transition or cross-over by means of heavy ion experiments, one ought to be concerned about non-equilibrium effects due to heating and cooling of the system. In this paper we extend our previous study of Glauber dynamics of 2D Potts models to the 3D 3-state Potts model, which serves as an effective model for some QCD properties. We investigate the linear theory of spinodal decomposition in some detail. It describes the early time evolution of the 3D model under a quench from the disordered into the ordered phase well, but fails in 2D. Further, the quench leads to competing vacuum domains, which are difficult to equilibrate, even in the presence of a small external magnetic field. From our hysteresis study we find, as before, a dynamics dominated by spinodal decomposition. There is evidence that some effects survive in the case of a cross-over. But the infinite volume extrapolation is difficult to control, even with lattices as large as 120^3 .

PACS numbers: PACS: 05.50.+q, 11.15.Ha, 25.75.-q, 25.75.Nq

I. INTRODUCTION

In a previous paper [1], which we denote by I in the following, we investigated the dynamics of 2D Potts models in the Glauber universality class. Dynamics in this class, model A in the classification of Ref.[2], contains local Monte Carlo (MC) updating schemes [3] which imitate the thermal fluctuations of nature. Here we extend our study to the 3D 3-state Potts model with and without an external magnetic field. This model gives an effective description of the deconfinement transition [4, 5, 6, 7] and by adding an external field [8], one can represent the effect of quark masses.

A detailed motivation of our study in the context of QCD and a compilation of preliminaries such as Potts models, spinodal decomposition, Fortuin-Kasteleyn (FK) clusters and structure functions, are given in the first two sections of I and are not repeated here. Hysteresis calculations for 2D Potts models are presented in I for a number of observables including the (internal) energy, properties of FK clusters and structure function. The main result is that the dynamics leads for most parameter values to a spinodal decomposition, which dominates the statistical properties of the configurations, independently of whether the equilibrium transition is second or first order. Hysteresis cycles and time evolution after a cooling [9] quench are presented in I and we find also initial evidence (compare Fig. 18 of I) that the scenario of dynamical spinodal decomposition may survive when the equilibrium transition is rendered into a cross-over. The latter point is of importance for QCD, because lattice simulations and effective models suggest that for physical quark masses m_u , m_d of the order of 10 MeV and m_s of the order of 150 MeV neither a chiral nor a deconfining transition occurs in the sense that there are thermodynamical singularities [10].

In the linear approximation of spinodal decomposition Cahn-Hilliard theory [11, 12] for model B predicts an exponential growth of the low momentum structure function in the initial part of the time evolution. Whether such an exponential growth was found or not was used by Miller and Ogilvie [13] to determine a critical k_c between low and high momentum modes, which they related to the Debye screening mass. In this paper we present the linear approximation, derive its diffusive differential equation, and confront the predicted exponential growth with MC data.

At the present level our results are mainly qualitative. Within a model of dynamics one expects universal properties, because the equations of motion differ only in their constants, but not in their general structure. The proper dynamics for Minkowskian relativistic dynamics is expected to be hyperbolic. Altogether little is known about the kind of effects one may expect to be produced by a dynamics. Therefore, we would like to advocate studies of different models of dynamics to get a handle on their similarities and differences. We begin with the diffusive dynamics of model A by the pragmatic reason that it is relatively easy to follow the time evolution of corresponding MC algorithms. The study of hyperbolic dynamics within full QCD or just pure non-Abelian gauge theory is presently out of reach. However the Polyakov loop model of Pisarski and Dumitru [14] allows for simulations in the Minkowskian [15] and it may be interesting to confront an investigation of its dynamics with our present results.

In the next section we fill a gap of the literature by presenting the linear theory of spinodal decomposition for model A. Our numerical results are compiled in section III, with quench and hysteresis investigations in subsections. Summary and conclusions are given in the final section IV.

II. SPINODAL DECOMPOSITION IN THE LINEAR APPROXIMATION

Metastable states are non-equilibrium states with lifetimes comparable to the time of observation, while unstable states are non-equilibrium evolving states with no observable lifetime [16, 17]. When dealing with metastable states we consider systems with a first order phase transition, while unstable states can be observed for systems with first and second order phase transitions.

Metastable and unstable states are distinguished by different types of instability characterizing the early stages of a phase separation. Metastable states require finite amplitude, localized fluctuations. The system evolves by growing the nuclei or droplets of the new phase and the theory of nucleation explains (e.g. Becker-Döring theory [16, 17]) the rate of formation of such nucleating droplets. In contrast, infinitesimal amplitude, non-localized fluctuations are sufficient for the initial decay of unstable states, which is called spinodal decomposition.

In mean field theory there is a sharp distinction between metastable and unstable states. They are separated by the spinodal curve, which is the locus of points inside the coexistence curve for which an appropriate susceptibility (for instance the concentration susceptibility $\partial c/\partial \mu$ for binary fluids) diverges. There is no sharp distinction in real systems.

There is a difference in the dynamics for models with conserved (model B in the classification of [2]) and non-conserved (model A) order parameters. Binary alloy or binary fluid models are typical examples of models with conserved order parameters (the concentration c). Originally [11, 12] the linear approximation was developed for model B. Following [18] we consider here a linear theory of spinodal decomposition for model A. Related results can also be found in [19]. The general picture is the same for model A and model B dynamics. The difference is in the quantitative details.

A. Coarse-grained free energy

We start by considering the coarse-grained free energy [11]. It is a functional of the order parameter and its minima correspond to the equilibrium states of the model. To use the coarse-grained energy for a study of non-equilibrium phenomena, one assumes that the model is not too far from equilibrium. The requirement is fulfilled for systems with slow dynamics on the scale of local equilibration times.

One introduces a spatial mesoscopic length scale l , separating the fast dynamics local microscopic regions from the slow dynamics macroscopic regions. The system is divided into regions (*elementary physical cells*) of size l , which are centered around vector coordinates \vec{r} defining their positions. The length scale l has to be significantly larger than the lattice spacing size, $l \gg a$, to allow for

a statistical treatment of the elementary physical cells. The other requirement is that $l \ll \xi$, where ξ is a typical correlation length of the system. On the scale l one treats the system as being in the equilibrium. The order parameter $m(\vec{r}, t)$ (e.g. the magnetization) has to vary smoothly on the length scales larger than l , to satisfy the requirement that the system on these length scales is not far from equilibrium.

Since elementary physical cells are equilibrated, their equilibrium thermodynamical functions are defined. We write down the coarse-grained partition function for the system of cells

$$Z_l(\{m\}) = \sum'_{\{S\}} \exp(-E\{S\}/k_B T), \quad (1)$$

where the sum is over spin configurations $\{S\}$ and the prime indicates the constraint

$$\frac{1}{l^d} \sum_{\{S\} \in \text{cell } \vec{r}_i} S_i = m(\vec{r}_i). \quad (2)$$

By summing in Eq. (1) over all configurations $\{m\}$ of magnetization, one gets the normal partition function.

The coarse-grained free energy is

$$F_l(\{m\}) = -k_B T \ln Z_l(\{m\}) = \int d^d r f(m(\vec{r})), \quad (3)$$

where we introduced the non-uniform free energy density $f(m(\vec{r}))$ and treat the magnetization as a continuous function of \vec{r} . We assume that f is a function of the local magnetization and its derivatives and expand it about f_0 , the free energy per spin of a uniform phase. For a cubic lattice $f(m, \nabla m, \dots) = f_0(m) + k_1 \nabla^2 m + k_2 (\nabla m)^2 + \dots$ and

$$F_l(\{m\}) \simeq \int d^d r [f_0(m) + k_1 \nabla^2 m + k_2 (\nabla m)^2]. \quad (4)$$

Applying Green's first identity [20] and imposing that ∇m is zero at the boundary, we obtain

$$\begin{aligned} \int d^d r k_1 \nabla^2 m &= - \int d^d r \nabla k_1 \nabla m \\ &= - \int d^d r \left(\frac{dk_1}{dm} \right) (\nabla m)^2. \end{aligned} \quad (5)$$

The coarse-grained free energy can be written as

$$F_l(\{m\}) = \int d^d r \left[\frac{1}{2} K (\nabla m)^2 + f_0(m) \right], \quad (6)$$

$$\text{where } \frac{1}{2} K = k_2 - \frac{dk_1}{dm}. \quad (7)$$

It has the familiar Ginzburg-Landau form. Note that f_0 depends on the choice of the spatial length scale l .

B. The linear approximation

The phenomenological model we use is based on the assumption that the rate of displacement of the order parameter is linearly proportional to the local thermodynamic force $\delta F/\delta m(\vec{r})$

$$\frac{\partial m}{\partial t} = -\Gamma \frac{\delta F}{\delta m(\vec{r})}. \quad (8)$$

The coefficient of the proportionality, Γ , is the response coefficient and defines the relaxation time scale of the system. This equation describes a purely dissipative system and not one with an internal Hamiltonian dynamics.

Let us determine the variation of the coarse-grained free energy (6)

$$\delta F_l(\{m\}) = \int d\vec{r} \left[\frac{1}{2} K \frac{d(\nabla m)^2}{d(\nabla m)} \delta \nabla m + \frac{df_0(m)}{dm} \delta m \right]. \quad (9)$$

Using again Green's first identity and dropping the surface integral, we write the variation as

$$\delta F_l(\{m\}) = \int d\vec{r} \left[-K \nabla^2 m + \frac{df_0(m)}{dm} \right] \delta m. \quad (10)$$

The functional derivative is

$$\frac{\delta F}{\delta m(\vec{r})} = -K \nabla^2 m + \frac{df_0(m)}{dm} \quad (11)$$

and the equation of motion becomes

$$\frac{\partial m}{\partial t} = -\Gamma \left[-K \nabla^2 m + \frac{df_0}{dm} \right]. \quad (12)$$

The Langevin approach [17] gives the same equation, but with a noise term added. We are interested in the fluctuations of the magnetization about some average value m_0

$$m(\vec{r}, t) = m_0 + u(\vec{r}, t). \quad (13)$$

To solve the differential equation we write it for small fluctuations

$$\begin{aligned} \frac{\partial u(\vec{r}, t)}{\partial t} \simeq \\ -\Gamma \left[-K \nabla^2 u(\vec{r}, t) + \frac{df_0(m_0)}{dm_0} + u(\vec{r}, t) \frac{d^2 f_0(m_0)}{dm_0^2} \right] \end{aligned} \quad (14)$$

and represent $u(\vec{r}, t)$ as a Fourier series

$$u(\vec{r}, t) = \frac{1}{V} \sum_{\vec{k}} \hat{u}(\vec{k}, t) \exp(i\vec{k} \cdot \vec{r}). \quad (15)$$

Using the Fourier series Eq. (14) becomes

$$\begin{aligned} \frac{1}{V} \sum_{\vec{k}} \left[\frac{\partial \hat{u}(\vec{k}, t)}{\partial t} - \omega(\vec{k}) \hat{u}(\vec{k}, t) \right] \exp(i\vec{k} \cdot \vec{r}) \\ = -\Gamma \frac{df_0(m_0)}{dm_0} \end{aligned} \quad (16)$$

$$\text{where } \omega(\vec{k}) = -\Gamma \left(K k^2 + \frac{d^2 f_0(m_0)}{dm_0^2} \right). \quad (17)$$

Multiplying both sides by $\sum_{\vec{r}} \exp(-i\vec{k}' \cdot \vec{r})$ and using the Kronecker function relation

$$V \delta(\vec{k} - \vec{k}') = \sum_{\vec{r}} \exp(i(\vec{k} - \vec{k}') \cdot \vec{r})$$

we get

$$\frac{\partial \hat{u}(\vec{k}', t)}{\partial t} - \omega(\vec{k}') \hat{u}(\vec{k}', t) = g(k') \quad (18)$$

$$\text{where } g(k) = -\Gamma \frac{df_0(m_0)}{dm_0} \sum_{\vec{r}} \exp(i\vec{k} \cdot \vec{r}). \quad (19)$$

The general solution is

$$\hat{u}(\vec{k}', t) = C \exp(\omega(\vec{k}') t) - \frac{g(\vec{k}')}{\omega(\vec{k}')}. \quad (20)$$

Except for the linear term this equation is the same as the one produced for model B by Cahn-Hilliard theory [11] and a similar analysis is appropriate. If

$$\frac{d^2 f_0(m_0)}{dm_0^2} > 0$$

holds, Eq. (17) implies that the amplitude of any fluctuation approaches a constant exponentially fast with time. But if the second derivative is negative, then one sees an exponential growth of the fluctuations for momentum modes smaller than the critical value

$$k < k_c = \left[-\frac{1}{K} \frac{d^2 f_0(m_0)}{dm_0^2} \right]^{1/2}.$$

C. Equation of motion for the structure factor

The structure factor (or function) can be measured in condensed matter experiments: A system is exposed to radiation of a wavelength λ and the scattering intensity at different angles θ is recorded. The structure factor $\hat{S}(\vec{k}, t)$ is proportional to the scattering intensity at the angle θ , where $k = (4\pi/\lambda) \sin(\frac{1}{2}\theta)$. In the gauge theory studies one may expect that the structure factor reflects the production of corresponding momentum gluons. The structure function can be written as

$$\begin{aligned} \hat{S}(\vec{k}, t) &= \int \langle u(\vec{r}, t) u(\vec{r}', t) \rangle \exp(i\vec{k} \cdot (\vec{r} - \vec{r}')) d\vec{r} d\vec{r}' \\ &= \langle \hat{u}(\vec{k}, t) \hat{u}(-\vec{k}, t) \rangle \end{aligned} \quad (21)$$

To derive the equation of motion for the structure factor we take the time derivative of $\hat{S}(\vec{k}, t)$ and make use of Eq. (18)

$$\begin{aligned} \frac{\partial \hat{S}(\vec{k}, t)}{\partial t} &= \langle 2 \hat{u}(\vec{k}, t) \hat{u}^*(\vec{k}, t) \omega(k) \rangle \\ &+ \langle (\hat{u}^*(\vec{k}, t) + \hat{u}(\vec{k}, t)) g(k) \rangle. \end{aligned} \quad (22)$$

The average of fluctuations about the average magnetization has to be zero $\langle \hat{u}(\vec{k}, t) \rangle = 0$. Thus (22) becomes

$$\frac{\partial \hat{S}(\vec{k}, t)}{\partial t} = 2\omega(\vec{k}) \hat{S}(\vec{k}, t), \quad (23)$$

with the solution

$$\hat{S}(\vec{k}, t) = \hat{S}(\vec{k}, t=0) \exp\left(2\omega(\vec{k})t\right). \quad (24)$$

We see that it is very similar to the evolution of fluctuations. Again, if $d^2 f_0(m_0)/dm_0^2 < 0$ low momentum modes grow exponentially. The value of the critical momentum is the same as for the fluctuations. The maximum growing mode is the one for which $\omega(\vec{k})$ takes on its maximum, $\omega_{\max} = \omega(k_{\max})$. In the linear theory $k_{\max} = 0$ according to Eq. (17). The values of $\omega(\vec{k})$ decrease with increasing k . Then there exists a k_c value, so that higher momentum modes $k > k_c$ are exponentially decaying. The results in the linear approximation are the same as for models with conserved order parameter, except for the values of $\omega(\vec{k})$ and k_{\max} .

A similar structure factor behavior may be obtained from the somewhat more accurate Langevin approach if we consider only linear terms. This result was first obtained for model B by H. Cook according to the review [17]. For model A a straightforward algebra yields

$$\frac{\partial \hat{S}(\vec{k}, t)}{\partial t} = 2\omega(\vec{k}) \hat{S}(\vec{k}, t) + 2k_B T \Gamma + 2g(k). \quad (25)$$

When the intrinsic dynamics of the system is prevailing over the extrinsic thermal fluctuations than the right hand side is dominated by the first term and the previous result for the structure function (24) is recovered.

D. Validity of the linear approximation

In the following we assume the existence of two phases, each described by a single equilibrium value of an order parameter. Potts models belong to a slightly more general group, because there are $q = 2, 3, \dots$ equilibrium values in the ordered phase. To trace them in our present discussion would lead to a rather cumbersome notation. Now the uniform free energy f_0 at the scale l has two minima which correspond to the equilibrium values of the order parameter in the two phases: m_1 and m_2 . The obvious criterium for the validity of the linear approximation is that the mean square value of fluctuations of the magnetization are much smaller than the square of the magnetization scale, $\Delta m = m_2 - m_1$: $\langle u^2 \rangle \ll (\Delta m)^2$.

Note that the fluctuations u depend on the introduced coarse-grained scale. The fluctuations are averaged over the cells of volume $l^d \sim k_c^{-d}$

$$\langle u^2(\vec{r}, t) \rangle = S(0, t) = \int d\vec{k} \hat{S}(\vec{k}, t) \sim k_c^d \hat{S}(0, t) \quad (26)$$

and we can write the condition for the validity of the linear approximation as

$$k_c^d \hat{S}(0, t) \ll (\Delta m)^2. \quad (27)$$

The Langevin approach allows us to estimate the value of $\hat{S}(0, t)$ from the requirement that the first term of the right-hand side of (25) is the largest (see [17] for similar consideration for model B) and gives

$$\frac{k_B T k_c^d}{|d^2 f_0(m_0)/dm_0^2| (\Delta m)^2} = \frac{k_B T k_c^{d-2}}{K (\Delta m)^2} \ll 1. \quad (28)$$

If we assume that the system is near the critical point T_c , this equation is *not* fulfilled. Close to T_c the only relevant length scale is the correlation length $\xi \sim k_c^{-1}$. The analysis of planar interfaces [17] shows that $K(\Delta m)^2/\xi$ is essentially a surface tension σ in a scaling sense. So we can rewrite (28) as

$$\frac{k_B T_c}{\sigma \xi^{d-1}} \ll 1. \quad (29)$$

But critical point scaling arguments show that the ratio $(k_B T_c)/(\sigma \xi^{d-1})$ is a universal constant of order unity for $d < 4$. This means that for near-critical quenches the linear approximation is not valid and non-linear behavior is relevant.

For quenches far from the transition point $T \ll T_c$ the mean-field approach becomes accurate. It allows to evaluate the condition (28) of validity of the linear approximation. Using mean-field estimates one finds inequality (28) to hold for both model A and B [21]:

$$\left(\frac{a}{\xi_0}\right)^d \left(\frac{T}{T_c}\right)^2 \left(1 - \frac{T}{T_c}\right)^{d/2-2} \ll 1, \quad (30)$$

where a is the lattice spacing and ξ_0 is the range of the interaction. For Potts models $a/\xi_0 = 1$. Eq. (30) is satisfied for $d < 4$ and $T \ll T_c$. Note the dependence on the number of dimensions in both limits considered.

III. NUMERICAL RESULTS

Our Boltzmann weights are $\exp(-\beta E)$ with the energy function

$$E = -2 \sum_{\langle \vec{r}, \vec{r}' \rangle} \delta_{\sigma(\vec{r}, t), \sigma(\vec{r}', t)} - 2h/\beta \sum_{\vec{r}} \delta_{\sigma(\vec{r}, t), \sigma_0}. \quad (31)$$

The first sum runs over all nearest neighbor sites \vec{r} and \vec{r}' , and σ takes the values $1, \dots, q$. In this paper we rely on symmetric lattices of $N = L^d$ spins in $d = 2$ and $d = 3$ dimensions.

Of the 3D zero magnetic field Potts models the $q = 2$ Ising model exhibits a second order phase transition, and the transitions are first order for $q \geq 3$. The model of our interest is the 3D 3-state model, which in zero magnetic field has a weak first-order phase transition at

$\beta_c = 0.275283(6)$. This transition persists for small values of the magnetic field h and has a second order endpoint at

$$\beta_c = 0.27469(1) \quad \text{and} \quad h_c = 0.000388(5) \quad (32)$$

as determined in Ref.[22] (there is a factor of two difference between our notation here and this reference).

The structure factor is (see I)

$$S(\vec{k}, t) = \frac{1}{N_s^2} \sum_{q_0=0}^{q-1} \left\langle \left| \sum_{\vec{r}} \delta_{\sigma(\vec{r}, t), q_0} \exp[i\vec{k}\vec{r}] \right|^2 \right\rangle. \quad (33)$$

Spinodal decomposition is characterized by an explosive growth in the low momentum modes, while the high momentum modes relax to their equilibrium values.

During our simulations the structure functions are averaged over rotationally equivalent momenta and the notation S_{k_i} is used to label structure functions of momentum $|\vec{k}| = k_i$ where

$$\vec{k} = \frac{2\pi}{L} \vec{n}. \quad (34)$$

In 2D we recorded the structure function for the modes: n_1 : (1, 0) and (0, 1), n_2 : (1, 1), n_3 : (2, 0) and (0, 2), n_4 : (2, 1) and (1, 2), n_5 : (2, 2).

In 3D we recorded the modes (including the permutations) n_1 : (1, 0, 0), n_2 : (1, 1, 0), n_3 : (1, 1, 1), n_4 : (2, 0, 0), n_5 : (2, 1, 0), n_6 : (2, 1, 1), n_7 : (2, 2, 0), n_8 : (2, 2, 1) and (3, 0, 0), n_9 : (3, 1, 0), n_{10} : (3, 1, 1), n_{11} : (2, 2, 2), n_{12} : (3, 2, 0), n_{13} : (3, 2, 1), n_{14} : (3, 2, 2), n_{15} : (3, 3, 0), n_{16} : (3, 3, 1), n_{17} : (3, 3, 2), n_{18} : (3, 3, 3). Note the accidental degeneracy in length for n_8 .

As in I we measured various properties of FK and geometrical clusters. See the definitions given in I.

For most of our simulations we use the heat bath algorithm with systematic updating, because we found previously that systematic updating is faster than random updating. However, for the linear theory of spinodal decomposition, one may be interested in the very early time development. Then it is advantageous to be able to take data within one sweep and we use random updating for a few cases.

A. Quench

We study the time evolution after a quench from an initial to a final temperature

$$T_{\text{initial}} \rightarrow T_{\text{final}} \quad (35)$$

and are interested in the limit of large lattices, $L \rightarrow \infty$. To get a statistically meaningful sample, we performed between 20×20 and 32×10 repetitions of each quench. Here the first number counts the PCs we used in parallel and the second number gives the repetitions performed on each PC.

The large number of repetitions required and the various adjustable parameters (T_{initial} , T_{final} and L) make a thorough investigation laborious and quite computer time consuming. Therefore, we were not able to arrive at conclusion for all questions, which deemed interesting to us.

1. Structure Functions

Miller and Ogilvie [13] investigated the dynamics of SU(2) and SU(3) gauge theories after quenching from a low to a high physical temperature (corresponding to the $\beta_{\text{min}} \rightarrow \beta_{\text{max}}$ in the spin system). They report a critical value k_c , so that modes grow (do not grow) exponentially for $k < k_c$ ($k > k_c$). Using an effective potential approach, they were able to relate k_c to the Debye screening mass.

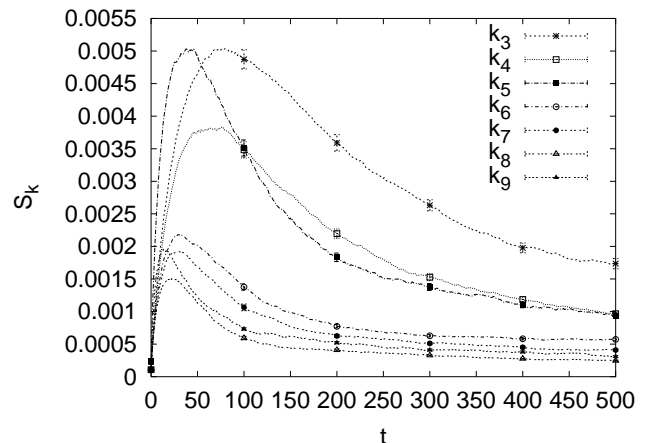


FIG. 1: Structure functions for the 2D Ising model quench $\beta = 0.2 \rightarrow 0.6$ at zero field on an 80×80 lattice.

First we give an example that our 2D Potts model data do not support the initial exponential growth predicted by the linear approximation. Fig. 1 depicts the $k \geq k_3$ structure function for the 2D Ising model quench $\beta = 0.2 \rightarrow 0.6$ at zero field on an 80×80 lattice (the modes k_1 and k_2 are omitted, because their peaks are more than four times higher than those of k_3 and k_4). As these functions do not show an initial exponential increase, random updating was subsequently used to be able to follow the time development within one sweep. Figure 2 shows the thus obtained very early time development of the structure functions of S_{k_i} for $i = 1, 2, 3$ and 4. The increase is linear in t . The curves turn then concave, excluding any exponential growth.

In Fig. 3 we plot our structure functions for a $\beta = 0.2 \rightarrow 0.3$ quench with sequential updating for the 3D 3-state Potts model. Their early time development allows for exponential fits of the form (24)

$$C_1(k) + C_2(k) \exp(2\omega(k)t). \quad (36)$$

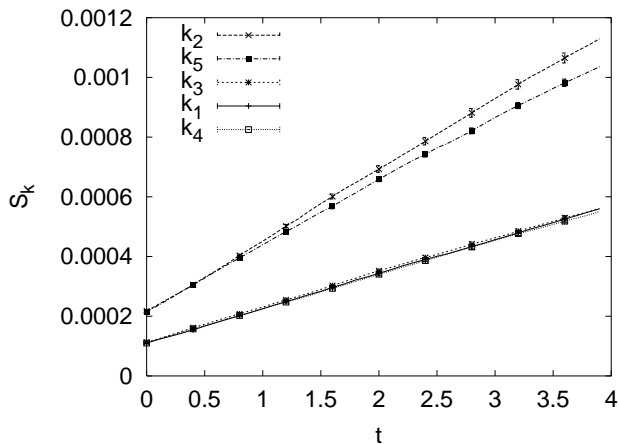


FIG. 2: Very early time evolution of the 2D Ising model quench $\beta = 0.2 \rightarrow 0.6$ at zero field on an 80×80 lattice. The order in the legend agrees with the order of the curves and the lower three curves fall almost on top of one another.

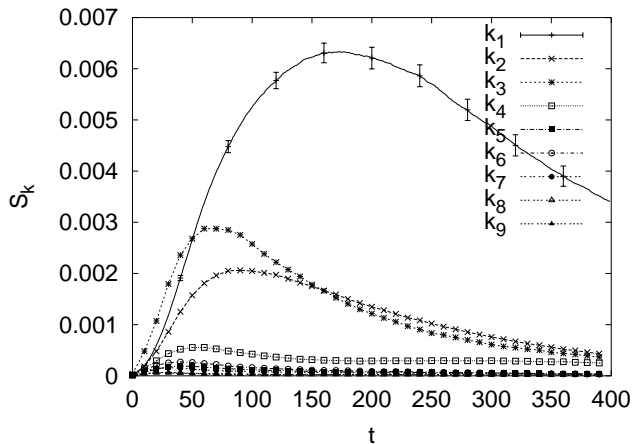


FIG. 3: Structure functions for the $\beta = 0.2 \rightarrow 0.3$ 3D 3-state Potts model quench at zero field on a 40^3 lattice.

In Fig. 4 we show the corresponding random and sequential updating data (the latter without error bars, not to overload the figure). The time between the updating schemes is scaled according to $t_{\text{rand}} = 1.94 t_{\text{seq}}$.

The fit values for $\omega(k)$ are positive for the low values of k_i , $i \geq 1$. Notably, the largest value ω_{max} is obtained for k_3 in contrast to the monotonous decrease of $\omega(k_i)$ which the linear theory (17) predicts for increasing k_i . Already our 2D results of Fig. 2 disagreed with the ordering of $\omega(k_i)$ predicted by the linear theory, but there it comes to no surprise, as the linear theory fails altogether in 2D. In 3D the k_3 mode appears to be the only major exception, amazingly already observed as such in pure gauge theory [13], from a picture which is over-all consistent with the predicted decrease of $\omega(k_i)$ for increasing k_i . The fits become quite unstable when $\omega(k)$ approaches zero. For even higher k_i values negative $\omega(k)$ values are obtained,

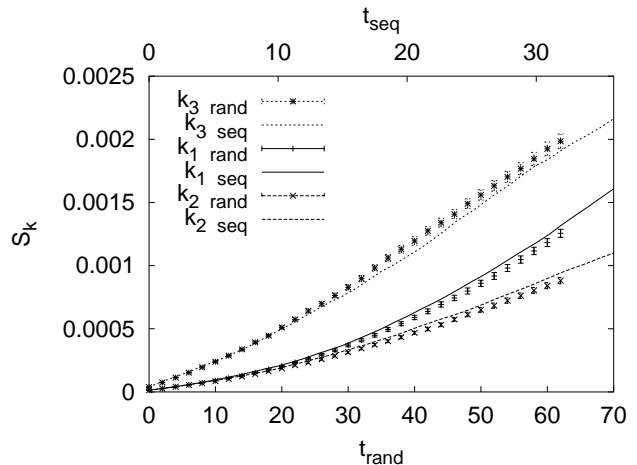


FIG. 4: The early time evolution for the quench of Fig. 3 together with random updating data. The order in the legend agrees with the order of the curves.

indicating an initial, exponential approach towards the constant $C_1(k)$, reaching for larger times a maximum and converting into a decrease on an always concave curve.

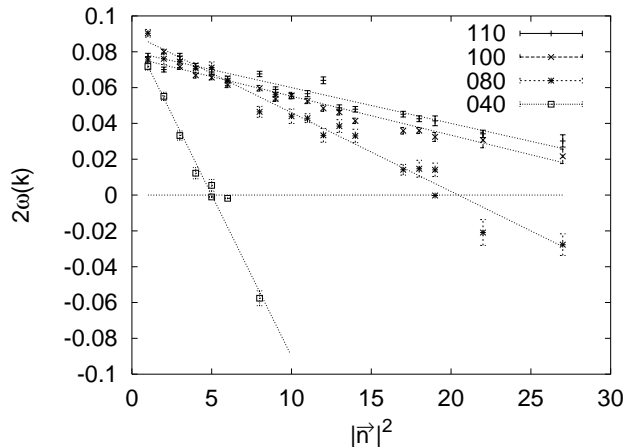


FIG. 5: Determination of k_c for the 3D Potts model at zero field.

For sequential updating we have pushed our analysis to L^3 lattices as large as $L = 110$. The results of all our $\omega(k)$ fits (36) are compiled in Fig. 5 versus $|\vec{n}|^2$ defined by equation (34). Approximately, we find straight lines $\omega(k) = a_0 + a_1 |\vec{n}|^2$ with a negative slope a_1 and we determine the critical momentum k_c as the value where $\omega(k)$ changes its sign. Using (34) we find $k_c \approx k_5 = 0.351$ ($L = 40$) and $k_c \approx k_{16} = 0.342$ ($L = 80$). So the finite size correction from $L = 40$ to $L = 80$ is about 3%. For $L = 100$ and 110 we estimate $|\vec{n}_c|^2 \geq 31$, outside the range where we took data. The k_c estimate of [13] (the Polyakov loops substituting for the Potts spins) does not consider finite size corrections, which future studies may reveal.

2. FK Clusters

A quench in the temperature changes instantaneously the bond probability of FK cluster configurations and observables such as the number of clusters, the mean volume and surface, the maximum volume, and maximum surface change considerably. Then the evolution proceeds smoothly.

The FK Potts clusters are similar to domains in a ferromagnet. For each of the possible magnetizations we define the largest cluster. When we quench into the ordered phase one magnetization will eventually take over. However, a-priori the system does not know which direction this is, because it is prepared in the disordered state where all directions are equally probable. Let us address the question how the system grows domains. There are two alternatives. (i) The system grows a cluster of a particular magnetization, while clusters of the other magnetizations decay right from the beginning. (ii) The system grows clusters in each direction of magnetization. At a later stage smaller clusters coalesce by statistical fluctuations and one of the directions emerges as dominant.

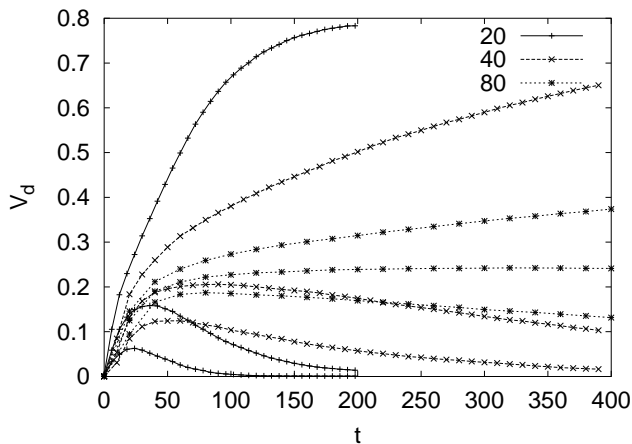


FIG. 6: Largest FK clusters of distinct magnetizations for the 3D 3-state Potts model quench $\beta = 0.2 \rightarrow 0.3$ at zero field on various size lattices.

In Fig. 6 we plot the evolution of the largest FK clusters for the three magnetizations of the 3-state Potts model in zero external magnetic field. For different lattice sizes the plot shows that the system grows clusters of each magnetization before one becomes dominant. The process of competitions between the largest clusters of different magnetization takes longer on the larger lattices.

To study the dependence of the speed of the evolution on the depth of the quench, we consider different final temperatures. In Fig. 7 we compile results for a 40^3 lattice and find that the growth of the largest clusters of all the magnetizations is faster when the system is quenched deeper into the ordered phase.

For gauge theories an equivalent percolation model

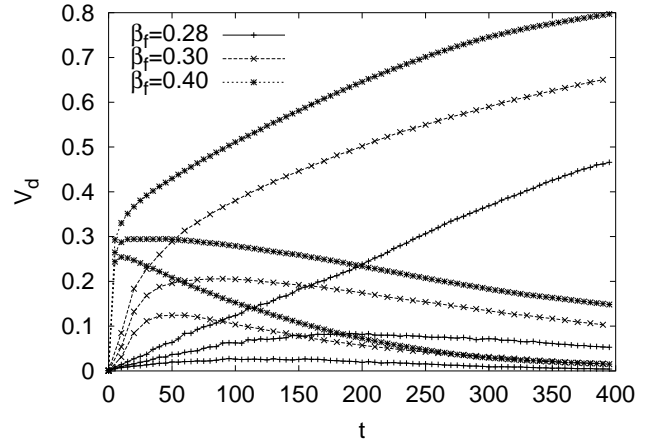


FIG. 7: Largest FK clusters of distinct magnetizations for the 3D 3-state Potts model quenches from $\beta = 0.2$ to β_f at zero external magnetic field on a 40^3 lattice.

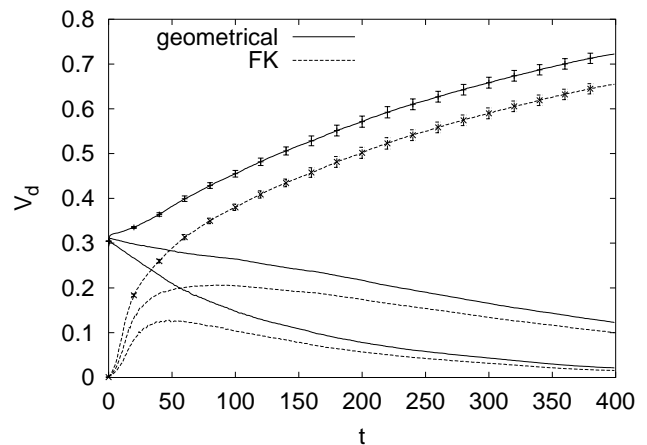


FIG. 8: Largest geometrical and FK clusters for the 3D 3-state Potts model quenched from $\beta = 0.2$ to $\beta_f = 0.3$ at zero field on a 40^3 lattice.

does not exist and it is problematic to find an appropriate substitute for the FK definition when clusters of Polyakov loops are considered. But it is easy to study geometrical clusters. Therefore, we compare for the 3D 3-state Potts model the evolution of geometrical and FK clusters in Fig. 8. The geometrical definition (bonds between neighboring spins of the same direction are always set) leads to the first of our two scenarios. Geometrical clusters do not compete. The system starts growing one of the domains, while reducing the largest domains of the other magnetizations right after the quench. This picture is unfavorable for the use of geometrical clusters of Polyakov loops in gauge theories. FK clusters are subsets of geometrical clusters. So, the FK clusters of the figure are always smaller than the geometrical. Sufficiently far in the ordered phase FK and geometrical domains converge in size, while closer to the disordered phase the

difference is significant, because geometrical clusters lead to artificial groupings of spins into clusters.

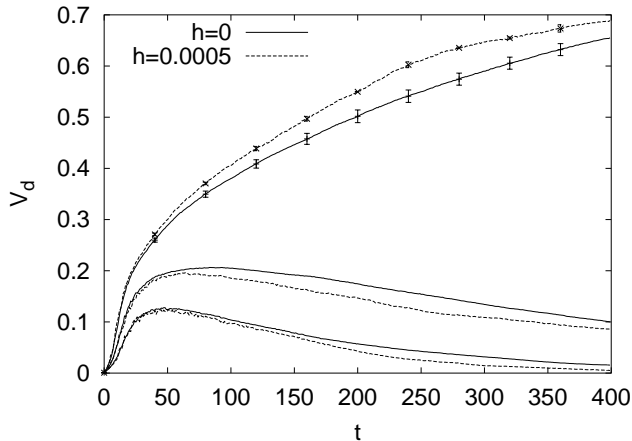


FIG. 9: The 3-D 3-state Potts model quenched from $\beta = 0.2$ to $\beta_f = 0.3$ at zero and $h = 0.0005$ external magnetic fields on a 40^3 lattice.

Next, we apply the external magnetic field $h = 0.0005$, which puts the model slightly above the critical endpoint at $h_c = 0.000388(05)$ in the $h-T$ plane, see Eq. (32), and drive the system through the emerging region of a sharp crossover. The external magnetic field sets the direction of preferable magnetization. In Fig. 9 we see that the growth proceeds in the same manner as for $h = 0$ with FK clusters of all magnetizations growing at the early time, only that the preferred domain grows a bit faster than before. This indicates that this effect may to some extent survive in QCD studies of the crossover region and finite size behavior in the $L \rightarrow \infty$ limit ought to be studied, although the physical volume relevant for RHIC experiments can only be approximated withing lattice gauge theory.

B. Hysteresis

In our 3D hysteresis investigation we look at the first order phase transition and rapid crossover region of the 3-state Potts model. We no longer study the limit of very slow dynamics (Eq. (7) of I), but use volume independent step-sizes

$$\Delta\beta' = \frac{2(\beta_{\max} - \beta_{\min})}{n'_\beta L_0^d}, \quad (37)$$

where L_0 is a constant used to set the scale. We chose $L_0 = 20$, which gives on a 20×20 lattice the same step-size as we used in I. The volume independent step-size (37) makes one sweep a physical time unit for model A type fluctuations in nature. It has the nice side effects that it allows to simulate larger volume lattices, but questions about the survival of effects in the limit of a slow dynamics become more difficult to answer.

We build ensembles of at least 160 cycles, grouped in bins of 20 cycles each. The error bars are obtained with respect to 32 jackknife bins for smaller lattices and 8 for larger lattices. The system is driven between $\beta_{\min} = 0.2$ and $\beta_{\max} = 0.4$. It is equilibrated in the disordered phase for at least 80 sweeps at β_{\min} , before being driven through a hysteresis cycle.

1. Latent Heat

As in I we use the maximum opening of the energy hysteresis as estimator for the latent heat on a finite lattice (some energy hysteresis pictures are given in I). Now we perform the limit $L \rightarrow \infty$ for a fixed dynamics defined by n'_β . The dynamics is at a constant speed in physical units, in contrast to the n_β dynamics used in I, which becomes infinitely slow in the limit of large lattices.

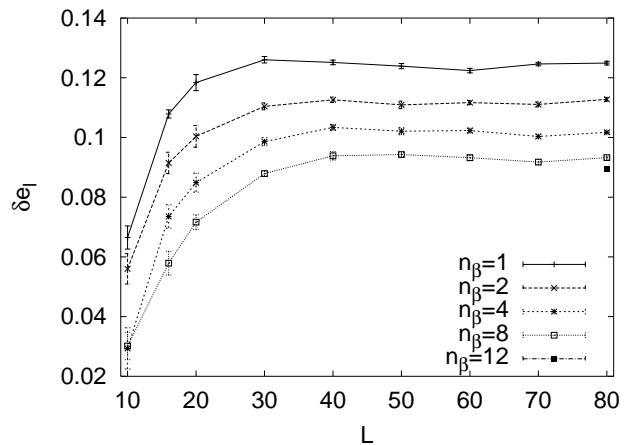


FIG. 10: The 3D 3-state Potts model finite size estimates of the latent heat for various n'_β dynamics at zero external magnetic field.

Relying on energy hysteresis curves for the 3D 3-state Potts model at zero external magnetic field, we plot in Fig. 10 the lattice size dependence of their maximum openings. A plateau is reached for $L \geq 30$ for the $n'_\beta = 1$ dynamics and for $L \geq 40$ for the large values of $n'_\beta = 4$ (slower dynamics). The error bars given in Fig. 10 are purely statistical and do not take into account a possible systematic error, which comes from the L independent constant step-size of the n'_β dynamics [25].

As plateaus for $\Delta\bar{e}_l(n'_\beta, L)$ are reached at $L \geq 40$, it is safe to take the $L = 80$ latent heat values as the our final answers. They are listed in the following. $n'_\beta = 1$: 0.1249 (7), $n'_\beta = 2$: 0.1128 (7), $n'_\beta = 4$: 0.1017 (5), $n'_\beta = 8$: 0.0932 (6), and $n'_\beta = 8$: 0.0895 (6). They are much larger than the equilibrium estimate $\Delta\bar{e}_l = 0.05354(17)$ [23]. The slower speed of the transition at higher n'_β lowers the values, but in the limit $n'_\beta \rightarrow \infty$ we still expect a dynamical latent heat which is larger than the equilibrium result. Namely, the $L \rightarrow \infty$

limit of the dynamics of I provides a lower bound and a dynamically generated latent heat was observed there for 2D Potts models, including the Ising model. In 3D one may want to modify the dynamics which gives a lower bound from $\Delta\beta \sim 1/V$ of I to $\Delta\beta \sim 1/L^2$, because the slowing down at the critical point of the Ising model scales with L^z and $z \approx 2$ (see Ref. [24] for estimates of z). Fitting our present $\Delta\bar{e}_l(n'_\beta)$ data to the form $\Delta\bar{e}_l(n'_\beta) = \Delta\bar{e}_l + a(n'_\beta)^b$ gives $\Delta\bar{e}_l = 0.057$ (9) with an exponent $b = -0.298$ (55). The rather large error bars prevent a conclusion about whether there is a dynamically generated latent heat in 3D or not. A change of the dynamics and/or a push towards larger n'_β values is required.

2. Structure Functions

The structure function behavior is similar to the 2D case with pronounced peaks in the cooling half-cycle. In Fig. 11 we plot S_{k_1} for the $n'_\beta = 1$ dynamics of the 3D 3-state Potts model in zero magnetic field. In Fig. 12 we show S_{k_1} in the external magnetic field $h = 0.0005$, which is slightly higher than the critical end-point field. Recall that k_i depends on the lattice size L through Eq. (34).

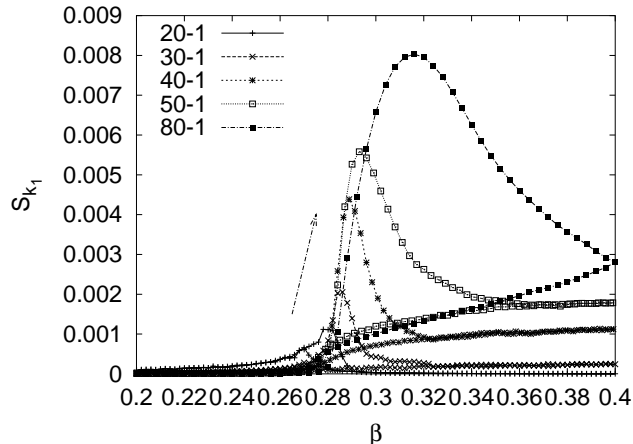


FIG. 11: Hysteresis of the structure function $S_{k_1}(\beta)$ on various L^3 lattices for the 3D 3-state Potts model in zero external magnetic field.

Arrows indicate the flow with increasing β . At $\beta = 0.4$ the hysteresis turns around and the lower curves describe the $\beta_{\max} \rightarrow \beta_{\min}$ approach. For the smaller lattices (most clearly for $L = 20$) they exhibit small peaks around the transition temperature, which are similar in size to peaks one finds for equilibrated configurations. For the larger lattices these peaks are not seen. Their returning curves come in too high, because their hysteresis are at $\beta = 0.4$ still far out of equilibrium.

As expected, the $\beta_{\min} \rightarrow \beta_{\max}$ peaks are smaller in the presence of the external magnetic field. While for $h = 0$ they increase over the entire range of our lattices, we find

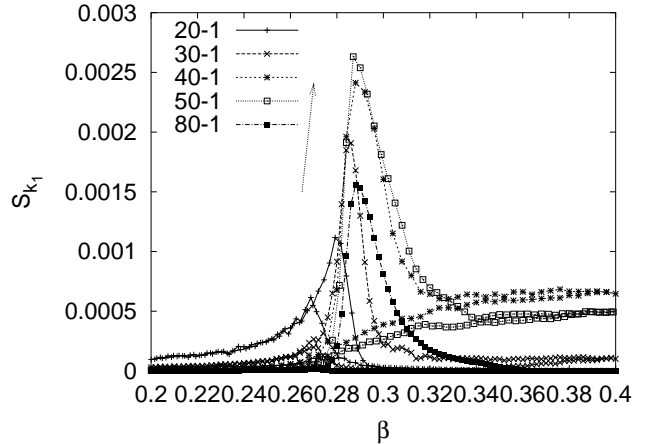


FIG. 12: Hysteresis of the structure function $S_{k_1}(\beta)$ on various L^3 lattices for the 3D 3-state Potts model in the external magnetic field $h = 0.0005$.

for $h = 0.0005$ an initial increase, which turns around between $L = 40$ and 60 . However, the subsequent decrease appears to be slow compared to non-critical behavior for which the structure functions S_{k_i} falls off $\sim 1/V$ in our normalization. Possibly, the behavior is similar to the equilibrium behavior at a second order phase transition point, where the fall-off is $\sim 1/L^x$ and $0 < x < 3$.

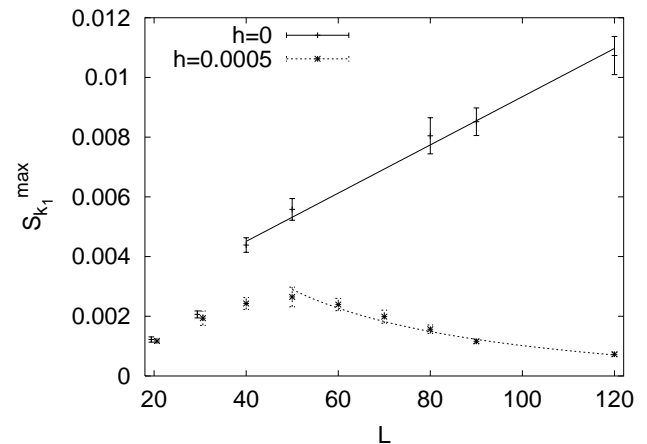


FIG. 13: Structure function S_{k_1} maxima versus lattice size for the $n'_\beta = 1$ dynamics of the 3D 3-state Potts without external magnetic field ($h = 0$) and in the cross-over region ($h = 0.0005$). For $L = 20$ and 30 the data points are slightly shifted, so that it becomes visible that there are results for both $h = 0$ and $h = 0.0005$.

Including lattices as large as 120^3 , we plot in Fig. 13 our estimates of the structure function maxima for S_{k_1} ($h = 0$ and $h = 0.0005$) together with fits for the larger lattices. Unfortunately, the precision of the data does not allow to determine the exponent x in a fit of the form

$$S_k^{\max} = a_1 + a_2 L^x \quad (38)$$

accurately. Choosing the exponent by hand, $x = +1$ for $h = 0$ and $x = -1$ for $h = 0.0005$, we find a satisfactory goodness-of-fit Q (for the definition of Q see, e.g., Ref. [26]) in each case. Using the non-critical $x = -3$ (instead of $x = -1$) to fit the $h = 0.0005$ data, gives the too small goodness-of-fit $Q = 0.0062$. Of course, this cannot exclude that the behavior turns to non-critical for even larger lattices. In this connection it is puzzling that the value $x = +1$ used to fit the $h = 0$ data cannot be asymptotic. In our normalization the S_k structure functions are bounded from above by $S_k \leq 1$, implying $x \leq 0$ for any true asymptotic behavior. Apparently lattices of size $L > 120$ are needed. With checkerboard updating they could be handled on supercomputers.

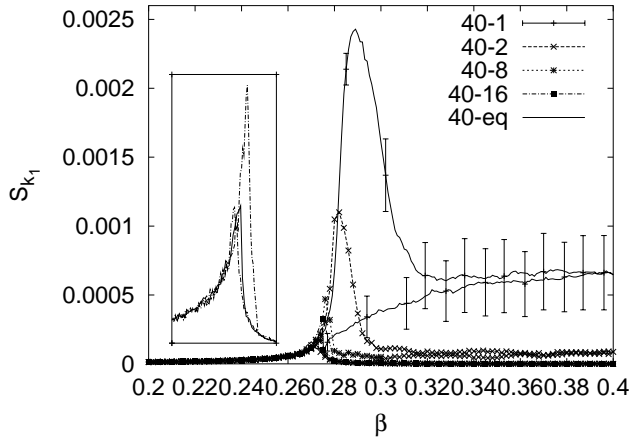


FIG. 14: The structure function S_{k_1} hysteresis for the 3D 3-state Potts model in the $h = 0.0005$ external magnetic field on a 40^3 lattice for simulations with the n'_β dynamics indicated by the extension to the lattice size. The inlay enlarges the equilibrium peak together with the slowest dynamics $n_\beta = 16$ data (β is mapped on $0.21 + 2(\beta - 0.26)$ and S_{k_1} on $4S_{k_1} + 0.0001$).

For a 40^3 lattice we plot in Fig. 14 the structure function S_{k_1} for the 3D 3-state Potts model in the $h = 0.0005$ field for different n_β up to 16 together with equilibrium data. The approach to equilibrium with the decrease of the speed of the dynamics (increase of n'_β) appears to be faster than in 2D. Possibly a greater connectedness of domains allows in higher dimensional models for a faster evolution of macroscopic structures. The heating ($\beta_{\max} \rightarrow \beta_{\min}$) peak develops and reaches the equilibrium peak, as we reduce the speed. The cooling peak decreases, but it would need much slower simulations to reach the equilibrium values. Thus within a range of speeds the cooling peak stays strong and spinodal decomposition is the dominant scenario. For $h = 0$ the figure looks very similar, but for an increase of all peak values by a factor of about two. The explanation of the difference between the heating and cooling branches presented for 2D models in I remains valid. Driven from the disordered to the ordered phase, the system freezes in domains of different magnetization, which are slow to

evolve. For a fast dynamics it does not have enough time to equilibrate in the ordered phase. The decrease of the speed allows then the system to equilibrate in the ordered phase and the heating peak emerges.

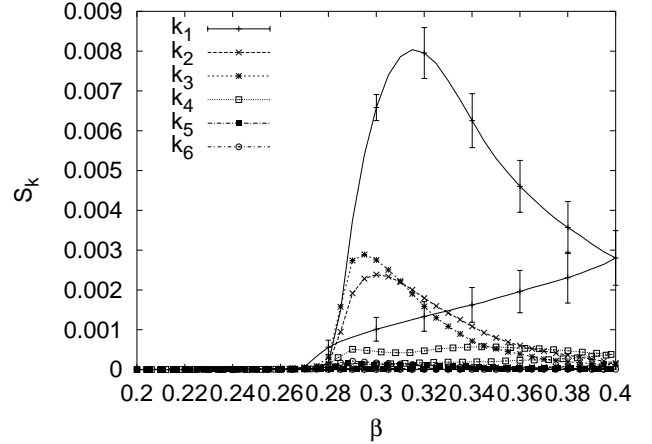


FIG. 15: Hysteresis for the structure functions for the 3D 3-state Potts model on an 80^3 lattice in zero external field.

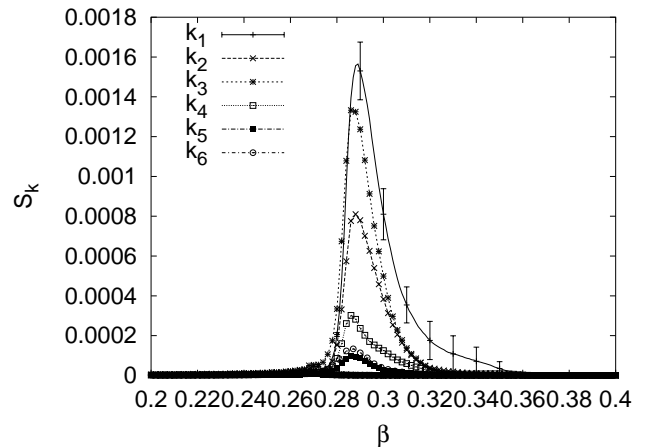


FIG. 16: Hysteresis for the structure functions for the 3D 3-state Potts model on an 80^3 lattice in the $h = 0.0005$ external field.

In Fig. 15 and 16 we plot for an $L = 80$ lattice the lowest momentum (k_1, \dots, k_6) structure functions for zero and non-zero external magnetic field. In the absence of the external magnetic field we observe that the peaks are very pronounced for k_1 to k_3 , and much smaller for $k \geq k_4$. In the presence of the external magnetic field all peaks are smaller and the difference between lower and higher modes is less distinct. We still observe a qualitative difference between the $k \leq k_3$ and the $k \geq k_4$ modes. Another observation is that the peaks are less broad for $h = 0.0005$ than for $h = 0$, because the system equilibrates for $h > 0$ easier in the ordered phase.

3. FK Clusters

In I we identified the maximum connected surface of FK clusters as an interesting quantity. In the transition region it exhibits a pronounced peak related to percolation. The 3D analysis [18] of this quantity has remained limited to rather small lattices ($L \leq 30$), because of a rapid slowing down with lattice size of the algorithm identifying the maximum connected surface. In contrast to 2D deviations from equilibrium appear relatively weak. A reason may be that the extra dimension adds new degrees of freedom to the surface. For the crossover region ($h = 0.0005$) the approach to equilibrium is illustrated in Fig. 17 by comparing the dynamics at different speeds (including a ‘super-fast’ $n'_\beta = 1/4$ choice) with equilibrated data. Notably the figure is practically identical for the $h = 0$ transition, reiterating that percolation happens for a crossover in quite the same way as for a proper transition [27].

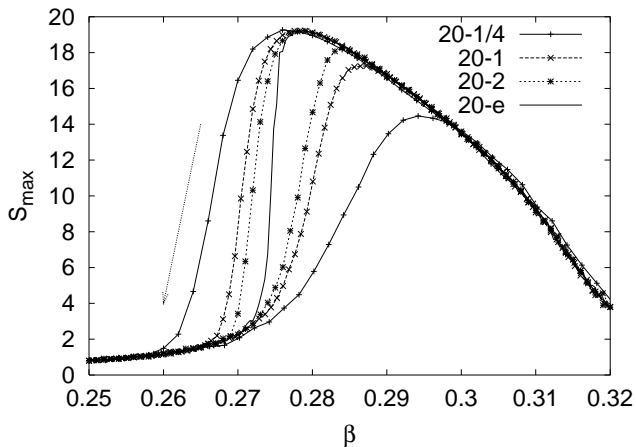


FIG. 17: Hysteresis for the largest connected cluster surface S_{\max} for the 3D 3-state Potts model in the external magnetic field $h = 0.0005$ on a 20^3 lattice. The hysteresis flow is indicated by the arrow. The n'_β values are given the extensions to the lattice size and e stands for equilibrium.

IV. SUMMARY AND CONCLUSIONS

In our simulations of the model A dynamics of the 3D 3-state Potts model on L^3 lattices, we find spinodal decomposition to be the dominant scenario of phase conversion. Under a quench from the disordered into the ordered phase, we observe an early time development of structure functions $S_k(t)$, which is in over-all agreement with the exponential growth predicted by the linear theory of spinodal decomposition for $k < k_c$ (Fig. 5). How-

ever, the ordering of the growth coefficients is not always in agreement with Eq. (17). Further, the linear approximation fails for near critical quenches (as was known before [17]) and, altogether, in 2D.

Following the structure function evolution over extended times, their pronounced peaks are the most noticeable feature. It is certainly a challenge to base a theory of spinodal decomposition on their finite size scaling instead of using the linear approximation. Unfortunately, very large lattices appear to be needed to extrapolate the infinite volume limit for the structure function maxima. Within our hysteresis investigation we pushed their analysis to systems as large as 120^3 . But, for zero external magnetic field we find an increase, which cannot yet be asymptotic, because it violates an upper bound. Applying a small external magnetic field ($h = 0.0005$) and quenching through the cross-over region results in an increase with L for small lattices ($L \leq 40$) and a *slower than non-critical* fall off on our larger ($L \geq 50$) lattices (Fig. 13). If the last trend continues towards $L \rightarrow \infty$, signals of spinodal decomposition would survive the continuum limit of an analogue QCD scenario.

A quench into the ordered phase leads to a competition of FK cluster domains. For the proper transition ($h = 0$) this leads to a divergence of the equilibration time in the limit $L \rightarrow \infty$, an effect well-known in condensed matter physics [28]. For a cross-over the $L \rightarrow \infty$ scenario is less scary, but our Fig. 9 shows that one may still expect a substantial time delay before reaching equilibrium. In the RHIC experiment one performs a near-critical quench into the quark-gluon plasma phase (assuming the phase is reached). For a near-critical quench FK clusters are initially small. In our Fig. 7 the largest one covers only about 10% the system. So, a number of vacuum domains are expected and the effects from the dynamics are manifested on their surfaces. Inside the domains the system may equilibrate fast, but the system as a whole cannot reach equilibrium easily. Unfortunately, a concise definition of FK clusters is not available for lattice gauge theory. Therefore, one may turn towards investigating directly the SU(3) gluonic energy density for influences of the supposedly underlying vacuum structure. First results will be published in Ref. [29].

Acknowledgments

BB and AV would like to thank Urs Heller and Michael Ogilvie for useful discussions. This work was in part supported by the US Department of Energy under contract DE-FG02-97ER41022. The simulations were performed on PC clusters at FSU and IUB.

[1] B.A. Berg, U.M. Heller, H. Meyer-Ortmanns, and A. Velytsky, Phys. Rev. D **69**, 034501 (2004).

[2] P.M. Chaikin and T.C. Lubensky, *Principles of con-*

- densed matter physics* (Cambridge University Press, Cambridge, 1997), table 8.6.1, p.467.
- [3] This includes all conventionally used Metropolis and heat bath updating schemes and not only the process proposed in R.J. Glauber, *J. Math. Phys.* **4**, 294 (1963).
- [4] B. Svetitsky and L.G. Yaffe, *Nucl. Phys. B* **210**, 423 (1982).
- [5] J. Bartholomew, D. Hochberg, P. H. Damgaard and M. Gross, *Phys. Lett. B* **133**, 218 (1983).
- [6] M. Ogilvie, *Phys. Rev. Lett.* **52**, 1369 (1984).
- [7] A. Gocksch and M. Ogilvie, *Phys. Rev. D* **31**, 877 (1985).
- [8] T. Banks and A. Ukawa, *Nucl. Phys. B* **225** [FS9], 145 (1983).
- [9] As in I we use the spin model notation for the temperature. Our cooling quench corresponds to the heating quench in laboratory deconfining experiments.
- [10] Z. Fodor and S.D. Katz, *J. HEP* **404**, 50 (2004) and **203**, 14 (2002); Ch. Schmidt, C.R. Allton, S. Ejiri, S.J. Hands, O. Kaczmarek, F. Karsch and E. Laermann, *Nucl. Phys. B. (Proc. Suppl.)* **119**, 517 (2003); F. Karsch, *AIP Conf. Proc.* **602**, 323 (2001); F. Karsch, E. Laermann, and Ch. Schmidt, *Phys. Lett. B* **520**, 41 (2001); F.R. Brown, F.P. Butler, H. Chen, N.H. Christ, Z. Dong, W. Schaffer, L.I. Unger, and A. Vaccino, *Phys. Lett. B* **251**, 181 (1990); H. Meyer-Ortmanns and B.-J. Schaefer, *Phys. Rev. D* **53**, 6586 (1996).
- [11] J.W. Cahn and J.E. Hilliard, *J. Chem. Phys.* **28**, 258 (1958).
- [12] J.W. Cahn, *Trans. Metall. Soc. AIME* **242** (1968) 166.
- [13] T.R. Miller and M.C. Ogilvie, *Nucl. Phys. B (Proc. Suppl.)* **106** (2002) 537; *Phys. Lett. B* **488** (2000) 313.
- [14] R.D. Pisarski, *Phys. Rev. D* **62** (2000) 111501(R); A. Dumitru and R. Pisarski, *Phys. Lett. B* **504** (2001) 282.
- [15] O. Scavenius, A. Dumitru and A.D. Jackson, *Phys. Rev. Lett.* **87** (2001) 182302
- [16] J.D. Gunton and M. Droz, *Introduction to the Theory of Metastable and Unstable States*, Springer, Berlin, 1985.
- [17] J.S. Langer in "Solids far from Equilibrium", C. Godreche (editor), Cambridge University Press, Cambridge, 1992.
- [18] A. Velytsky, Ph.D. thesis, Florida State University, Tallahassee, 2004. On the web at <http://etd.lib.fsu.edu>.
- [19] G. Brown and P. Rikvold, *Phys. Rev. E* **65**, 036137 (2002). This reference as well as Ref. [2] avoid to use the notion "spinodal decomposition" for model A (in contrast to model B). However, we follow Ref. [13], where the notion "spinodal decomposition" was used for model A type dynamics of lattice gauge theory.
- [20] J.D. Jackson, *Classical Electrodynamics*, Second Edition, Wiley & Sons, New York, 1975.
- [21] Equations (7.21) ff. of Ref. [17].
- [22] F. Karsch and S. Stickan, *Phys. Lett. B* **488**, 319 (2000).
- [23] N. Alves, B.A. Berg and R. Villanova, *Phys. Rev. B* **43**, 5846 (1991). Note that an extra factor 3/2 is used in the energy notation of the article.
- [24] D. Landau and K. Binder, *A Guide to Monte Carlo Simulations in Statistical Physics*, Cambridge University Press, Cambridge, 2000.
- [25] The constant step-size introduces slight problems in determining the precise location of the maximum (which in our dynamics of I went away for large L). This difficulty may lead to systematic errors, which could be overcome by using the slower random updating and taking data within a sweep. We did not do so as the systematic uncertainty appears to be smaller than the statistical. In particular, it decreases for increasing n'_β .
- [26] W.H Press, S.A. Teukolsky, W.T. Vetterling, and B.P. Flannery, *Numerical Recipes in Fortran 77*, Second Edition, Cambridge University Press, Cambridge, 1992.
- [27] H. Satz, *Comp. Phys. Commun.* **147** (2002) 40, and references given therein.
- [28] See p.484 of Ref. [2].
- [29] A. Bazavov, B.A. Berg, and A. Velytsky, in preparation.